Experimental and Numerical Study on The Boundary Layer Flow over a Flat Plate with a Semi-Circular Bump with and without a Transversal Wire

Sutardi Sutardi[1], Radiaprima Kartika Wijaya[1], Setyo Hariyadi[2]

[1]*Institut Teknologi Sepuluh Nopember Surabaya, Indonesia*
[2]*Politeknik Penerbangan Surabaya, Indonesia*

Corresponding author: sutardi@me.its.ac.id

Abstract. Flow behavior over a bump attached on a flat plate has significant effect on the total drag. The drag comprises of pressure and friction or viscous drags. Attaching a disturbance on the bump surface affects significantly on the contribution of pressure and viscous drag. This study is intended to examine the effect of a small wire (tripping wire) attachment on a semi-circular bump surface on the flow characteristics over the semi-circular bump. Special attention of this study is to examine the drag characteristics, pressure distribution, and boundary layer separation point from the bump surface.

The study was conducted using experimental and numerical methods. The experiments were conducted in a low-speed wind tunnel at a freestream velocity of 16.5 m/s, corresponding to the flow Reynolds number (Re) of approximately 2.1 x 105. Flat plates with a semi-circular bump with and without wire were attached in the wind tunnel test section used as model tests. The wire is attached at three different angle (θ) locations of the bump surface, namely θ = 30 deg, 40 deg, and 50 deg. The pressure distribution on the plate surface as well as on the bump surface is measured using static pressure taps connected to U-tube manometer. From the pressure distribution, then the pressure drag is obtained from the integration of pressure distribution on the surface. Fluid velocity is measured using a Pitot static tube. Numerical studies was conducted using a commercial software the Fluent. A 2-D, steady flow turbulent model k-ω shear-stress transport (SST) was used in this study. In the numerical simulation, the grid independency test is performed to ensure better results.

The results of the study show that the presence of a small wire attached on the bump surface increases to the total drag of the model for all values of θ. Also, the boundary layer separation point on the bump surface for all values of θ occurs at smaller angle comparing to that of the bump without wire. Results from the experimental study compare very well to the results obtained from the numerical simulations with a maximum difference of approximately 5 percent. In this study, the maximum drag occurs for the bump with the tripping wire attached at θ = 50 deg.

Keywords: *bump, boundary layer, separation*

Numerical Study of Three-Dimensional Flow Characteristics Around the Wing Airfoil E562 With Forward and Rearward Wingtip Fence

Setyo Hariyadi Suranto Putro[1], Sutardi Sutardi[2], Wawan Aries Widodo[2]

[1]*Politeknik Penerbangan Surabaya, Indonesia*
[2]*Institut Teknologi Sepuluh Nopember, Indonesia*

Corresponding author: hudzaifahsetyo@gmail.com

Abstract. Airfoil is an aerodynamic model that is widely used both on aircraft wings, Unmanned Aerial Vehicle (UAV) and fluid machines such as pumps, compressors and turbines. Airfoil on aircraft wings with the resulting lift force is used to lift the entire aircraft. The pressure difference between the top and bottom of the airfoil on the wing causes the plane to gain lift. Increased performance of the airfoil on the wing can be done in various ways, one of which is adding a winglet to reduce drag. It is expected that with an increase in lift and a decrease in drag force will increase the performance of the aircraft. This research was conducted by numerical simulation using Ansys 19.0. with turbulent model k-ω SST. The freestream flow rate used is 10 m / s (Re = 2.3 x 104) with the angle of attack (α) = 0°, 2°, 4°, 6°, 8°, 10°,12°,15°, 16°,17°,19° and 20°. The specimen model is an Eppler 562 (E562) airfoil with and without a winglet. From this study, tip vortex were seen in plain wings at high speeds and at rearward wingtip fence with lower speeds. In the area that has been separated (wake) which is indicated by a lower speed in plain wing x = 1c. In the z = 1.5c area, it is shown that there is a pathline difference between the three models showing the influence of the three-dimensional flow on the rearward wingtip fence where there is a higher velocity in the upper surface area. In the trailing edge z = 1.9 shows that there is a pathline from the lower surface to the upper surface in the plain wing and rearward wingtip fence.

Keywords: *airfoil, eppler 562, forward wingtip fence, rearward wingtip fence, tip vortex, winglet*

Numerical study of three-dimensional flow characteristics around the wing airfoil E562 with forward and rearward wingtip fence

Cite as: AIP Conference Proceedings 2187, 020017 (2019); https://doi.org/10.1063/1.5138272
Published Online: 10 December 2019

Setyo Hariyadi Suranto Putro, Sutardi, and Wawan Aries Widodo

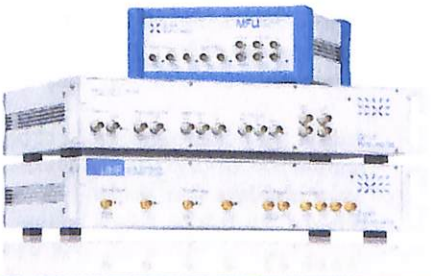

Numerical Study of Three-Dimensional Flow Characteristics Around the Wing Airfoil E562 With Forward and Rearward Wingtip Fence

Setyo Hariyadi Suranto Putro[1, a)], Sutardi[2, b)], and Wawan Aries Widodo [2, c)]

[1]*Aviation Polyteclmic of Surabaya, Surabaya, Indonesia*
[2]*Fluid Mechanic Laboratory, Mechanical Engineering Department, FTI, ITS, Surabaya, Indonesia*

[a)]hudzaifahsetyo@gmail.com
[b)]sutardi@me.its.ac.id
[c)] wawanaries@me.its.ac.id

Abstract. Airfoil is an aerodynamic model that is widely used both on aircraft wings, Unmanned Aerial Vehicle (UAV) and fluid machines such as pumps, compressors, and turbines. The airfoil on aircraft wings with the resulting lift force is used to lift the entire aircraft. Therefore, the researchers concentrate more on wing modification so that the resulting lift is more optimal.. Increased performance of the airfoil on the wing can be done in various ways, one of which is adding a winglet to reduce drag. It is hoped that a large enough lift and drag ratio will improve aircraft performance. This research was conducted by numerical simulation using Ansys 19.0. with turbulent model k-ω SST. The velocity flow rate used is 10 m / s (Re = 2.3 x 10^4) with α = 0°, 2°, 4°, 6°, 8°, 10°,12°,15°, 16°,17°,19° and 20°. The test model is an Eppler 562 (E562) airfoil with and without a winglet. From this study, tip vortex was seen in plain wings, forward wingtip fence and rearward wingtip fence with lower speeds. In the area that has been separated (wake) which is indicated by a lower speed in the three configurations x = 1c. In the z = 1.5c area, it is shown that there is a pathline pattern difference between the three configurations. It is shown that the influence of the three-dimensional flow on the rearward wingtip fence where there is a higher velocity in the upper surface area. In the trailing edge, z = 1.9 shows that there is a pathline from the lower surface to the upper surface in the plain wing and rearward wingtip fence. Keywords: wing, Eppler 562, winglet, tip vortex, forward wingtip fence, rearward wingtip fence

INTRODUCTION

The aerodynamic efficiency and drag of an airplane wing shape not only depend on the pressure drag but also induced drag or parasite drag due to lift. Induced drag is produced by the characteristics of three-dimensional airflow near the wingtip of the aircraft. When the flow meets at the wingtips, it will produce vorticity flow at the tip known as trailing vortices. Vortex flow at the wingtips of the aircraft can reduce the effectiveness of the lift force. The vortex that occurs behind the wing reduces the effective area of the upper side wing. In transportation by airplane, the main goal is to maximize profits by connecting the use of aircraft and wings. This can be done in several ways, namely by increasing the lift that will result in increased profits, reducing drag will reduce fuel consumption, reduce the weight of the wing by using a new material that will increase profits. Various configurations have been tried in various ways by researchers. The geometry that was formed was not as conventional as the past and even experienced a modification. This is as done by Kody et al (1) and El Haddad (2).

Hossain, A., et al, (3) was evaluated wing performance, the multi-winglet design to show the potential for further performance. It is shown that multi-winglet reduced parasite drag and improved aerodynamics performance around 15-30% compared to plain wing NACA 0012. In Europe, it is known as Wing-Grid which is a multiple wing configuration that is added to the wingtip. These small geometries are added at various angles so that the wingtip vortices do not interact to form a strong vortex. These smaller vortices waste energy from the vortex so that the lift distribution can be renewed and the wing induced drag reduced.

Innovative Science and Technology in Mechanical Engineering for Industry 4.0
AIP Conf. Proc. 2187, 020017-1–020017-8; https://doi.org/10.1063/1.5138272
Published by AIP Publishing. 978-0-7354-1934-6/$30.00

Dimino et al (4) made a preliminary study of winglets that could adjust to the load of the aircraft. The design of the winglets in this study was combined with the use of a flap on the trailing edge. This research also combining the sweep angle, the twist angle, the chord extension and the cant angle in some part of the wing. With a good initial design, research can reduce induced drag in the use of civil aircraft.

Wei et al (5) used the NACA 0012 airfoil in a study comparing several characteristics of fluid flow. This study shows that optimized winglets reduce the presence of three-dimensional flow at the joint between the winglet and wing. Besides, the comparison of vorticity between plain wing, winglet, and winglet which is optimized shows that winglet which is optimized with cant angle can reduce vorticity magnitude area.

Panagiotou et al (6) investigated the concept of morphing winglets on Medium Altitude Long Platform Endurance Unmanned Aerial Vehicles (MALE UAV) through CFD. Seven different cant angle configurations are examined in three predefined flight segments, multiple attack angles, and RANS equations. The results of this study indicate that the concept of winglet morphing can be used to perfect UAV flight performance with long durability, according to the needs of various demand mission segments.

Hariyadi et al (7) conducted a study of winglets on the use of unmanned aerial vehicles (UAVs). This research was used the turbulent model k-ω SST. Freestream flow velocity that used is 10 m / s ($Re = 2.34 \times 10^4$) with $\alpha = 0°$, 2°, 4°, 6°, 8°, 10°, 12°, 15°, 16°, 17° and 19°. Winglets that used are wingtip fence with forward and rearward variations. From the research, it was found that the winglets can reduce the vorticity magnitude and irregular velocity pathline behind the wing. Forward wingtip fence configuration results in the smallest area of vorticity magnitude than the other configuration. Also, the addition of a forward wingtip fence can reduce the growth of fluid flow jumps from the trailing edge more perfectly.

From the description above it can be seen that research in the field of UAV aerodynamics is still very wide open space to explore discoveries and improve the aerodynamic performance of the UAV. In this study, an Eppler 562 type airfoil will be used as an end wall attached to the wing. Wingtip fence with the forward and rearward configurations will be attached to the wing to see in detail the effect of the wingtip fence to the velocity vector, velocity pathline, and velocity magnitude.

RESEARCH METHODOLOGY

COMPUTATIONAL FLUIDS DYNAMIC

This research was conducted by numerical simulation using Ansys 19.0 with turbulent model K-ω SST. The freestream flow rate used is 10 m / s ($Re = 2.34 \times 10^4$) with $\alpha = 0°$, 2°, 4°, 6°, 8°, 10°,12°,15°, 16°,17°,19° and 20°. The model specimen is an E562 airfoil with variations in the use of winglets. The winglet that will be used is a forward and rearward wingtip fence. The Reynolds Number is determined based on the length of the chord. In this case, the chord length used is 20 cm. Fig. 1 represents the simulation domain and the boundary conditions used in the simulation.

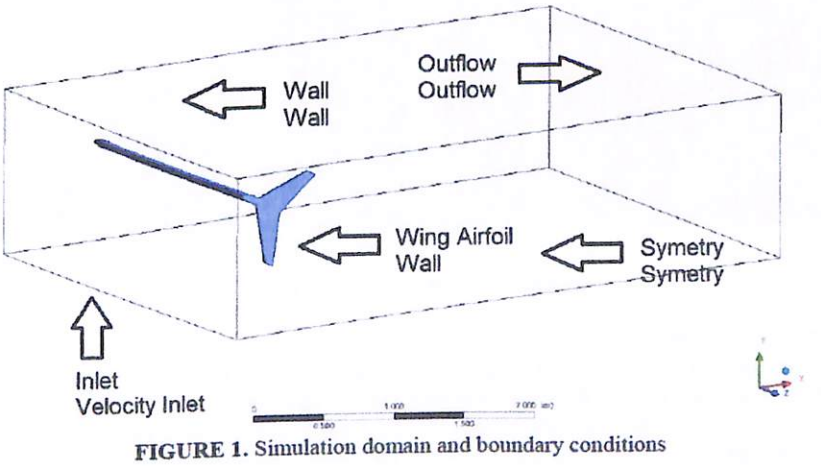

FIGURE 1. Simulation domain and boundary conditions

The test configuration is shaped in the form of an Eppler 562 type airfoil with and without a winglet in the form of a wingtip fence as shown in Fig. 2 and the dimensions of the modeling dimensions in Fig. 3 [7]. While the meshing used in this simulation study is shown in Fig. 4.

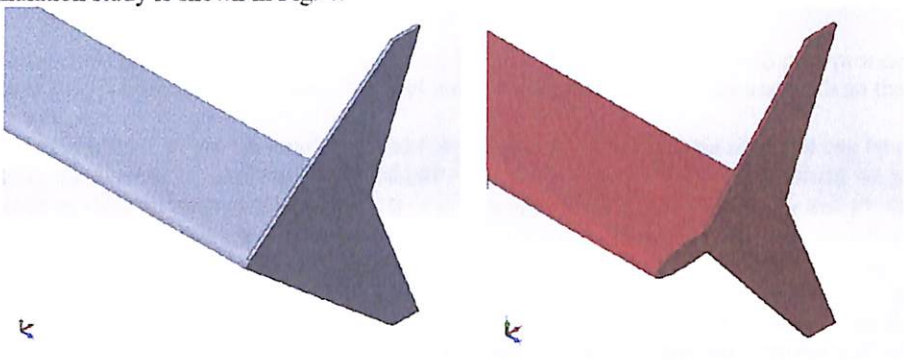

(a) Forward Wingtip Fence (b) Rearward Wingtip Fence

FIGURE 2. Specimens Model

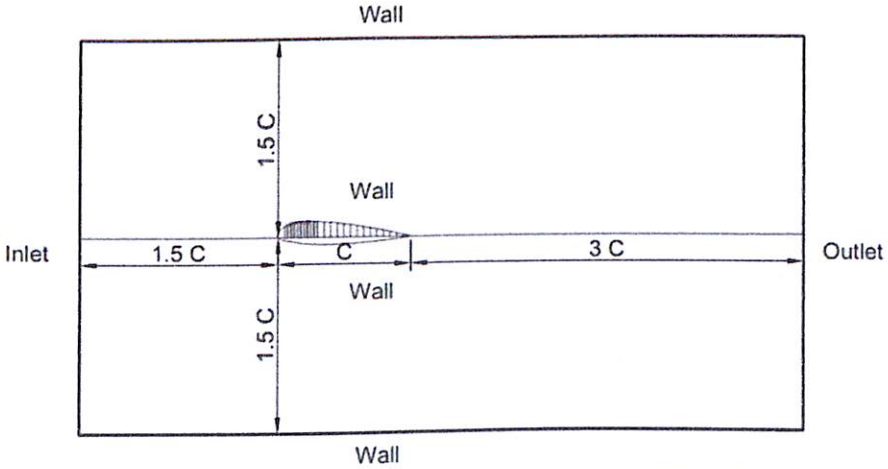

FIGURE 3. Modeling dimensions and background conditions (8)

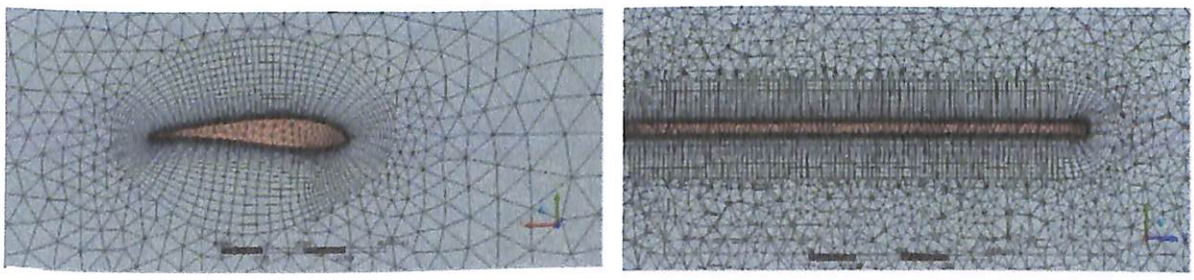

FIGURE 4. Geometry and meshing

The type and properties of the material are used at a temperature of 30 °C and a pressure of 1 atm. This model uses air as a working fluid with (ρ) = 1.17 kg / m3, viscosity (μ) = 1.86 x 10^{-5} N.s / m2. The turbulence intensity in this modeling simulation is 0.8% and the length scale of the inlet side is 0.024 m. The turbulent model used is viscous turbulent model k-ω SST. The solution criteria of the Ansys 19.0 use a turbulent kinetic energy-momentum, turbulent dissipation rate, and second order for pressure. Convergence criteria are set at 10^{-5}, meaning that the iteration process on the Ansys 19.0 is declared to have converged after the residual reaches a price less than 10^{-5}.

Grid Independency

The use of simulation software requires data accuracy both in the pre-processing and post-processing steps. The grid independence step is needed to determine the level and structure of the most efficient grids so that the modeling results are close to true.

Grid independence is done to get the amount of meshing that tends to be constant so that it can be obtained in this independence grid, the number of meshing is divided into 4 types, then from this type of meshing we will look for the smallest difference in value of each meshing by comparing the numerical C_D graph. The C_D and $y+$ value of the grid independency in the numerical simulation is shown in table 1. Table 1 shows the meshing variations of the three-dimensional grid independency of the test model at the Reynolds number 2.34×10^4. To get more complete information on the area around the wall, it requires the calculation of $y+$ on each meshing. In addition to the calculation of $y+$, the inflation layer is needed so that the area around the wall uses a type of quadrilateral meshing so that information around the wall is more accurate. To calculate the smaller number of nodes, the area far from the wall will use meshing tetrahedrons.

TABLE 1. Analysis of the three-dimensional E562 grid model without winglets

Number of *Meshing*	Number of *Nodes*	*Inflation Layer*	C_D	y^+
Meshing A	469.682	40	0,8588	2,1
Meshing B	768.081	40	0,8833	1,4
Meshing C	569.313	40	0,90198	0,8
Meshing D	353.120	40	0,9207	2,1

In this study, to get the best results, the $y+$ used is less than 1, as was done in the Kontogiannis (9) research. Based on table 1. C_D values that tend to be smaller occur in Meshing C. One of the considerations in using numerical simulations is the time and memory used, then the meshing used for comfortable simulations is Meshing C.

In this modeling, the flow characteristics step, including the selection of the solver model and determining the turbulence model are used. The solver model used is unsteady. The turbulence model used for this airfoil is the k-ω SST model.

The k-ω SST model developed by Menter to combine the formulation of a stable and accurate k-ω standard model in the area near the wall with the k-ε model which has advantages in freestream flow. To achieve this, a k-ω SST model was made. (10)

RESULT AND DISCUSSION

Velocity Vector

In Fig. 5, it is shown that velocity vector visualization comparison of the plain wing, forward wingtip fence, and rearward wingtip fence. When the velocity moves from an angle of 90° to 270°, the velocity strength is higher. But when velocity moves from 270° to 90° it has a lower value. In Fig. 5. (a) it is shown that the plain wing has a high-velocity density value at x = 0.5c. In figure 5 (b) it is shown that at x = c, the velocity density has decreased but still has a high value. This is indicated by the resulting velocity vector length. In figure 5 (c), the forward wingtip fence cant angle 90° produces The forward wingtip fence cant angle 90o produces velocity vector that congregates around the fence and the vector density is more tightly than the plain wing. A similar phenomenon occurs in Fig. 5 (d) which shows the velocity vector decreases. However, at rearward wingtip fence cant angle 90° at α = 17°, it produces the lowest velocity pattern compared to plain wing and forward wingtip fence. This is possible because there is a flow leak around the leading edge that is larger than the forward wingtip fence. This flow leakage not only causes a decrease in speed around the rearward wingtip fence but also causes an irregular flow pattern as shown in Fig. 5 (e). In Fig. 5 (f) it can be seen that irregular flow patterns behind the wing into the direction of the wingspan. The flow pattern from the bottom side controverts with the airflow from the top side. This results in a decrease in the velocity value at the rearward wingtip fence.

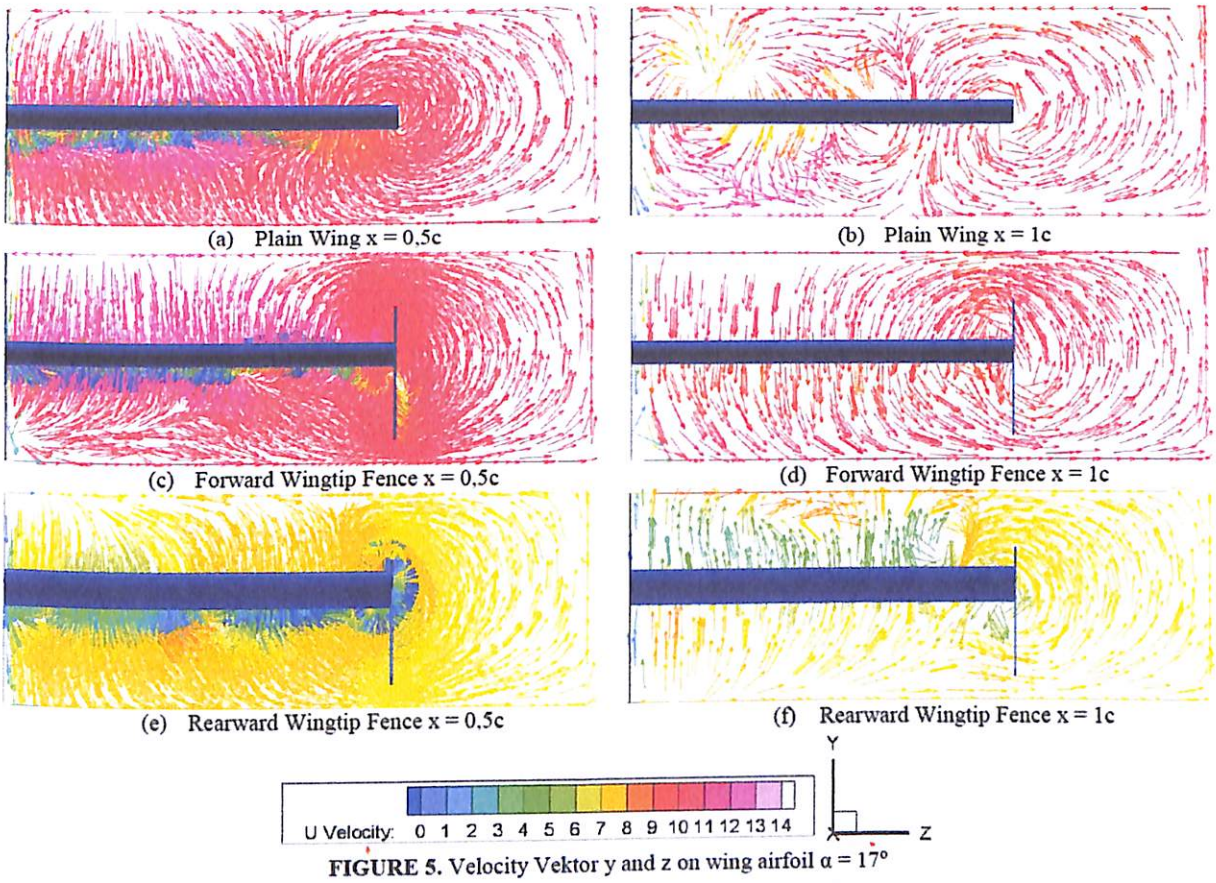

FIGURE 5. Velocity Vektor y and z on wing airfoil $\alpha = 17°$

Velocity Pathline

Fig. 6 shows the velocity contour along with the pathline of the flow passing through the plain wing Eppler 562 and with the winglets, at $\alpha = 17°$. It is seen from the cut in the midspan and the area near the tip ($z / s = 0.9$). It can be seen that the visualization of the velocity pathline and contours value in each variation show a certain pattern.

At $\alpha = 17°$, there is a difference in the phenomenon of flow passing through the airfoil midspan. On the Eppler 562 airfoil with a forward wingtip fence (Fig. 6 (c)) it has a wake phenomenon that occurs slightly smaller than the plain wing Eppler 562 (Fig. 6 (a)). Rearward wingtip fence configuration has a smaller wake region than forward wingtip fence configuration but larger than the plain wing. (Fig. 6 (e)). However, the plain wing and rearward wingtip fence have a slight velocity pathline that collides with the wake. It is suspected that this is the effect of leaps in fluid flow from the lower surface to the upper surface. The effect of this fluid flow jump is seen in the $z = 0.9$ area both on the plain wing (Fig. 6 (b)) and on the rearward wingtip fence (Fig. 6 (f)). But this does not occur in the forward wingtip fence. This shows that the influence of fluid flow jumps from the lower surface to the upper surface is felt up to the midspan region. But the result of the flow jump is influenced by the shape of the end wall in the wingtip area.

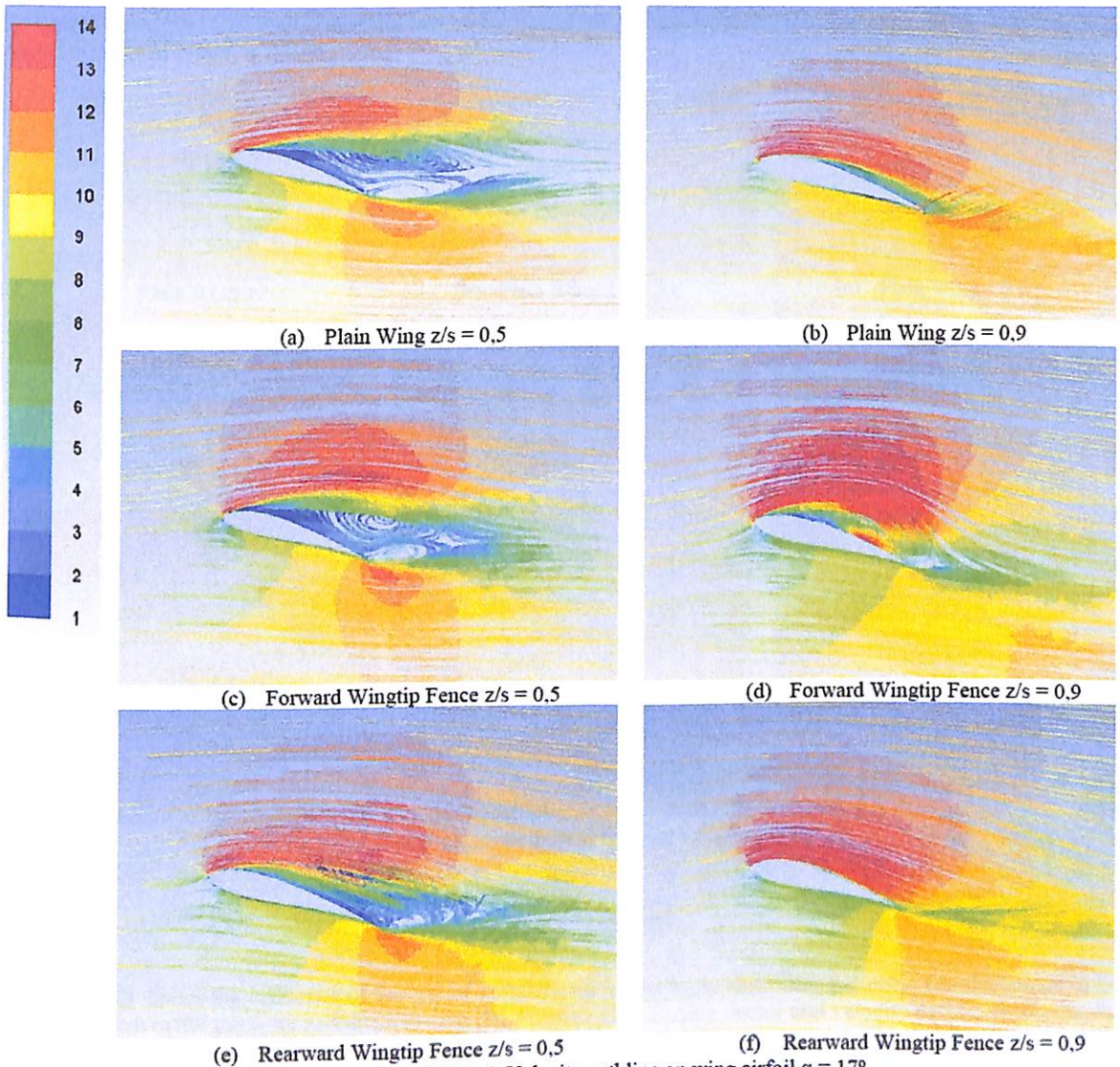

(a) Plain Wing z/s = 0,5 (b) Plain Wing z/s = 0,9

(c) Forward Wingtip Fence z/s = 0,5 (d) Forward Wingtip Fence z/s = 0,9

(e) Rearward Wingtip Fence z/s = 0,5 (f) Rearward Wingtip Fence z/s = 0,9

FIGURE 6. Velocity pathline on wing airfoil $\alpha = 17^{\circ}$

Velocity Magnitude

To observe the flow phenomenon in the tip region, velocity contours are observed in an isometric view of a particular y-z plane. It can be seen from Fig. 7 that tip vortex develops when the flow is at greater x / c. This is the following numerical studies conducted by Wells (2009). To facilitate the analysis of the vortex tip phenomenon in each configuration, the contours are only compared to x / c = 1, 1.5, and 2. In addition to facilitating analysis, all configurations show the same pattern where the magnitude of the tip vortex is greater at a large x / c. The illustration also displays velocity magnitude in the y and z directions to clarify the tip vortex phenomenon.

Fig. 7 gives information on the airflow of the trailing edge that moves from the lower side to the upper side. The airflow forms a vortex called the tip vortex. This is caused by pressure magnitude value on the upper side is smaller than the lower side so that the fluid jump to the tip of the wing. In the plain wing, it is pointed out that the tip vortex phenomenon is relatively larger than two other configurations. The tip vortex then shrinks at a greater distance from the wing. Similar tip vortex phenomena also occur in other configurations. Tip Vortex was arisen a small size develop with the shape of the end wall. However, in the forward wingtip fence and rearward wingtip fence, it can be seen that the contour is redder (velocity increases) around the airfoil in addition to the wake area. In areas that have been

dispersed (wake), the area with blue color increases. This phenomenon indicates that the wake region is getting bigger when the angle of attack is raised.

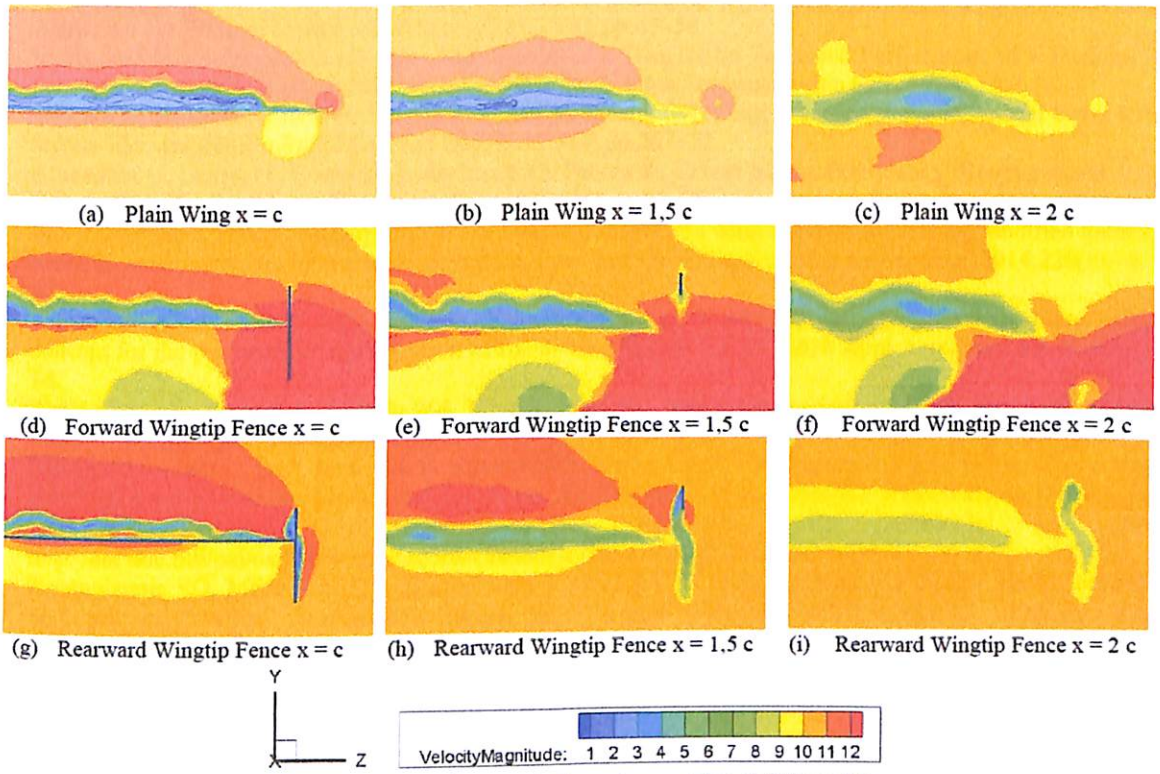

FIGURE 7. Velocity magnitude contour on wing airfoil $\alpha = 17°$

CONCLUSION

This study shows the influence of the use of winglets significantly on fluid flow patterns. The difference in flow patterns is seen in the midspan and the area near the winglet. The velocity vector and velocity pathline contours show this effect. From the numerical simulation, several fluid characteristics are shown, including:

- Fluid flow leaps affect the velocity vector value and density patterns. The geometry configuration of the rearward wingtip fence causes a decrease in the value and density of the velocity vector compared to the plain wing and forward wingtip fence.
- The plain wing has the highest velocity vector value and density compared to other geometric configurations.
- The effect of a fluid flow jump (tip vortex) has an impact that reaches the fold including in the form of the wake. Wake formed from plain wing shows the lowest value and wider area compared to other configurations. The use of winglets can reduce wake wide, especially in midspan areas. In the wingtip region, the fluid flow jumps from the lower surface to the upper surface.
- The addition of winglets influences the size of the wake in the midspan area and the size of the vortex tip behind the wingtip. Adding winglets will reduce wake size and tip vortex.
- The reduction in wake means reducing the induced drag generated from the E562 airfoil.

REFERENCES

1. Kody F, Bramesfeld G, Schmitz S. An Efficient Methodology for Using a Multi-Objective Evolutionary Algorithm for Winglet Design. Tech Soar. 2013;37(3), pp.45–56.
2. El Haddad N. Aerodynamic and Structural Design of a Winglet for Enhanced Performance of a Business Jet Scholarly Commons Citation. 2015;112. Available from: https://commons.erau.edu/edt/265
3. Hossain A, Rahman A, Hossen J, Iqbal P, Shaari N, Sivaraj GK. Drag reduction in a wing model using a bird feather like winglet. Jordan J Mech Ind Eng. 2011;5(3),pp.267–72.
4. Amendola G, Dimino I, Concilio A, Andreutti G, Pecora R, Cascio M Lo. Preliminary design process for an adaptive winglet. Int J Mech Eng Robot Res. 2018;7(1),pp.83–92.
5. Wei Z, Meijian S. Design optimization of aerodynamic shapes of a wing and its winglet using modified quantum-behaved particle swarm optimization algorithm. Proc Inst Mech Eng Part G J Aerosp Eng. 2014;228(9):1638–47.
6. Panagiotou P, Efthymiadis M, Mitridis D, Yakinthos K. A CFD-aided investigation of the morphing winglet concept for the performance optimization of fixed-wing MALE UAVS. 2018 Appl Aerodyn Conf. 2018,pp.1–14.
7. Setyo Hariyadi SP, Sutardi, Widodo WA, Mustaghfirin MA. Aerodynamics analisys of the wingtip fence effect on UAV wing. Int Rev Mech Eng. 2018;12(10).
8. Mulvany N, Chen L, Tu J, Anderson B. Steady-State Evaluation of Two-Equation RANS (Reynolds-Averaged Navier-Stokes) Turbulence Models for High-Reynolds Number Hydrodynamic Flow Simulations. Dep Defence, Aust Gov [Internet]. 2004;1–54. Available from: http://oai.dtic.mil/oai/oai?verb=getRecord&metadataPrefix=html&identifier=ADA426359
9. Kontogiannis SG, Mazarakos DE, Kostopoulos V. ATLAS IV wing aerodynamic design: From conceptual approach to detailed optimization. Aerosp Sci Technol [Internet]. 2016;56:135–47. Available from: http://dx.doi.org/10.1016/j.ast.2016.07.002
10. Harinaldi, Budiarso, Tarakka R, Simanungkalit SP. Effect of active control by blowing to aerodynamic drag of bluff body van model. Int J Fluid Mech Res. 2013;40(4):312–23.

Experimental and numerical study on the boundary layer flow over a flat plate with a semi-circular bump with and without a transversal wire

Cite as: AIP Conference Proceedings 2187, 020039 (2019); https://doi.org/10.1063/1.5138294
Published Online: 10 December 2019

S. Sutardi, Radiaprima Kartika Wijaya, and Setyo Hariyadi

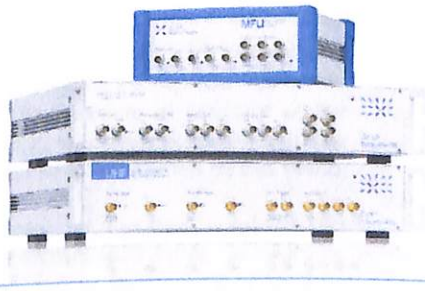

Experimental and Numerical Study on The Boundary Layer Flow over a Flat Plate with a Semi-Circular Bump with and without a Transversal Wire

S. Sutardi[1, a)], Radiaprima Kartika Wijaya[1], and Setyo Hariyadi[2,b)]

[1]*Mechanical engineering Dept., FTI-ITS, Surabaya, Indonesia.*
[2]*Aviation Polytechnic of Surabaya, Surabaya, Indonesia.*

[a)]Corresponding author: sutardi@me.its.ac.id
[b)] hudzaifahsetyo@gmail.com

Abstract. Flow behavior over a bump attached on a flat plate has significant effect on the total drag. The drag comprises of pressure and friction or viscous drags. Attaching a disturbance on the bump surface affects significantly on the contribution of pressure and viscous drag. This study is intended to examine the effect of a small wire (tripping wire) attachment on a semi-circular bump surface on the flow characteristics over the semi-circular bump. Special attention of this study is to examine the drag characteristics, pressure distribution, and boundary layer separation point from the bump surface. The study was conducted using experimental and numerical methods. The experiments were conducted in a low-speed wind tunnel at a freestream velocity of 16.5 m/s, corresponding to the flow Reynolds number (*Re*) of approximately 2.1 x 10^5. Flat plates with a semi-circular bump with and without wire were attached in the wind tunnel test section used as model tests. The wire is attached at three different angle (θ) locations of the bump surface, namely θ= 30 deg, 40 deg, and 50 deg. The pressure distribution on the plate surface as well as on the bump surface is measured using static pressure taps connected to U-tube manometer. From the pressure distribution, then the pressure drag is obtained from the integration of pressure distribution on the surface. Fluid velocity is measured using a Pitot static tube. Numerical studies was conducted using a commercial software the Fluent. A 2-D, steady flow turbulent model k-ω shear-stress transport (SST) was used in this study. In the numerical simulation, the grid independency test is performed to ensure better results. The results of the study show that the presence of a small wire attached on the bump surface increases to the total drag of the model for all values of θ. Also, the boundary layer separation point on the bump surface for all values of θ occurs at smaller angle comparing to that of the bump without wire. Results from the experimental study compare very well to the results obtained from the numerical simulations with a maximum difference of approximately 5 percent. In this study, the maximum drag occurs for the bump with the tripping wire attached at θ= 50 deg.

INTRODUCTION

Fluid flow passes over a bump experiences changes in velocity and pressure. At the upstream side of the bump surface, the velocity of fluid increases, while its pressure decreases. On the contrary, at the downstream of the bump midspan, the fluid pressure increases, while its velocity decreases. The increase in pressure at the downstream side of the bump is one of the causes of the boundary layer separation, where the momentum of the fluid is so small that cannot be able to overcome the pressure rise and the wall shear stress or friction on this bump. The penalty of this flow separation is the drag force on the bump.

There have been many studies related to boundary layers developing over bumps, such as study conducted by Wijanarko [1]. The study showed that there is a massive flow separation on the semicircular bump. In addition, Wijanarko's study showed that there was the influence of flow Reynolds number (*Re*) on the location of the flow separation point on the surface of the semi-circular bump. Moreover, Joongnyon and Hyung [2] evaluated the

Innovative Science and Technology in Mechanical Engineering for Industry 4.0
AIP Conf. Proc. 2187, 020039-1–020039-8; https://doi.org/10.1063/1.5138294
Published by AIP Publishing. 978-0-7354-1934-6/$30.00

phenomenon of pressure fluctuations within the turbulent boundary layer developing over a bump. Hadi [3] conducted a study on the effect of the radius of curvature of the semi-circular bump on the location of the flow separation point. This study showed that the location of the point of flow separation in a semi-circular bump with the radius of curvature at the wall-body junction (the line of contact between the bump and the flat plate) is able to delay separation.

Based on the above studies, it is intended to conduct a study of fluid flow over a semi-circular bump disturbed by a transverse wire (tripping wire) mounted on the upstream surface of the bump. This study is also motivated by the study of Werle [4] about the flow behavior on a sphere modified using a ring. The main objective of this study is to evaluate experimentally and numerically the effect of the placement of a tripping wire/rod on the semicircular bump surface on the boundary layer separation and the resulted total drag.

RESEARCH METHODS

Experimental and numerical simulation were used in this study. Experimental study was performed in a low-speed wind tunnel. Figure 1 shows the low-speed windtunnel used in this study, while Fig. 2 shows a flat plate and the semicircular bump with all dimensions. The pressure distribution on the plate surface as well as on the bump surface is measured using static pressure taps connected to U-tube manometer. Also, the velocity measurements were performed using Pitot static tube connected to U-tube manometer. A calibrated pressure transducer is also available to obtain pressure distribution in the flow field. The experimental studies were performed in a low-speed wind tunnel at a freestream velocity of 16.5 m/s, corresponding to the flow Reynolds number (Re) of approximately 2.1 x 10^4. Flow turbulence intensity at the test section centerline is approximately 0.8% at the velocity used in this study.

The numerical method was performed using Gambit and Fluent commercial softwares, the, where the turbulent model of k-ω shear-stress transport (SST) was used in this study. The simulation was carried out using two dimensional (2D) and steady flow mode. Several steps were carried out in this simulation: geometric modeling, grid generation, determining the analysis area and boundary conditions, iteration processes, and post processing. In the numerical simulation, the grid independency test follows the method of Mulvany et al [5]. Figure 3 shows the grid, the analysis area, and the boundary conditions used in this study, while Fig. 4 shows mesh enlargement around the bump. Table 1 shows simulation procedures and flow condition setting used in this study. All fluid properties are set to be similar or at least almost the same to that used in the experiments.

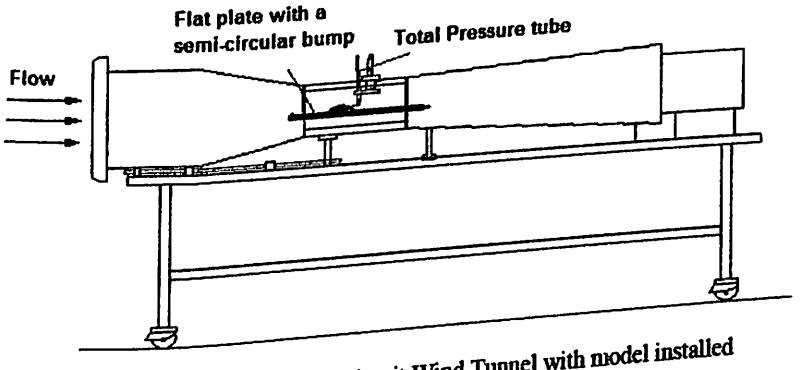

FIGURE 1. Subsonic Open Circuit Wind Tunnel with model installed

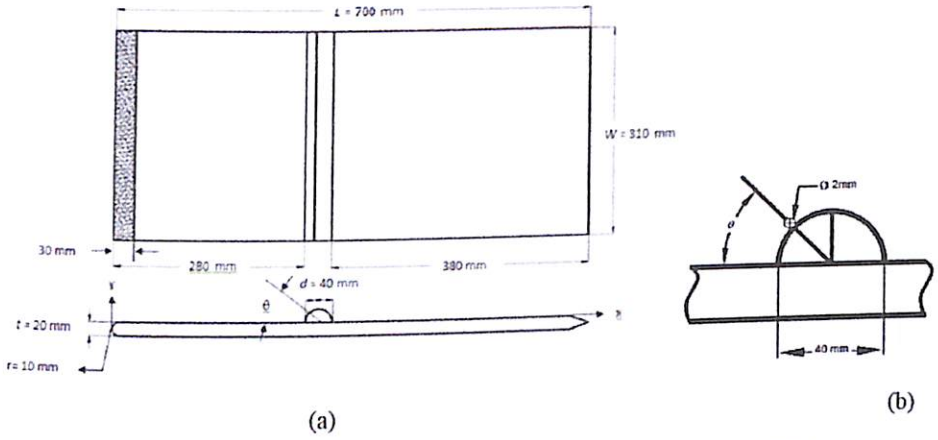

FIGURE 2. (a) Flat plate with bump: (b) bump with a tripping wire (rod).

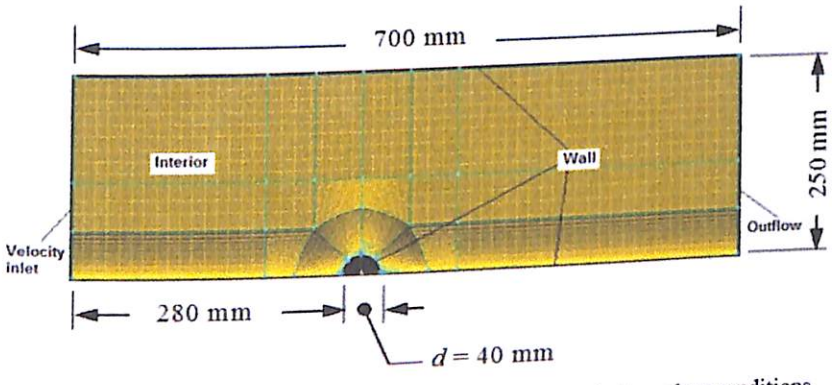

FIGURE 3. Simulation domain showing the location with the boundary conditions.

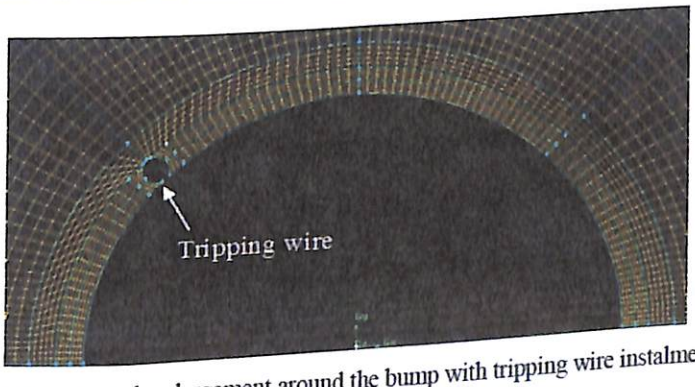

FIGURE 4. Mesh enlargement around the bump with tripping wire instalment.

TABLE 1. Simulation procedures and flow condition setting

Steps		Input
Boundary Conditions	Upper wall, lower wall, bump, and tripping wire	Wall
	Inlet	Velocity inlet (16.5 m/s)
	Outlet	Outflow
	Interior	Interior
Turbulent Model		k-ω SST
Material	Density (ρ)	1.18 kg/m^3
	Viscosity (μ)	1.85 x 10^{-5} kg/m.s
Operating Condition		STP Temperature = 28° C Pressure = 10^5 Pa
Solution		SIMPLEC and Second Order
Monitor Residual		10^{-6}

RESULTS AND ANALYSIS

Figure 5 shows the distribution of Cp in bumps without wire as a function of θ. The flow is accelerated due to strong favorable pressure gradient at the upstream side of the bump. This can be seen from the experimental and numerical results. Furthermore, the flow is slowed down, indicated by the increase in pressure (adverse pressure gradient) up to $\theta \sim 105°$. Beyond this point, the bump surface pressure becomes relatively constant, and the flow is predicted to have the boundary layer separation followed by flow relaxation process.

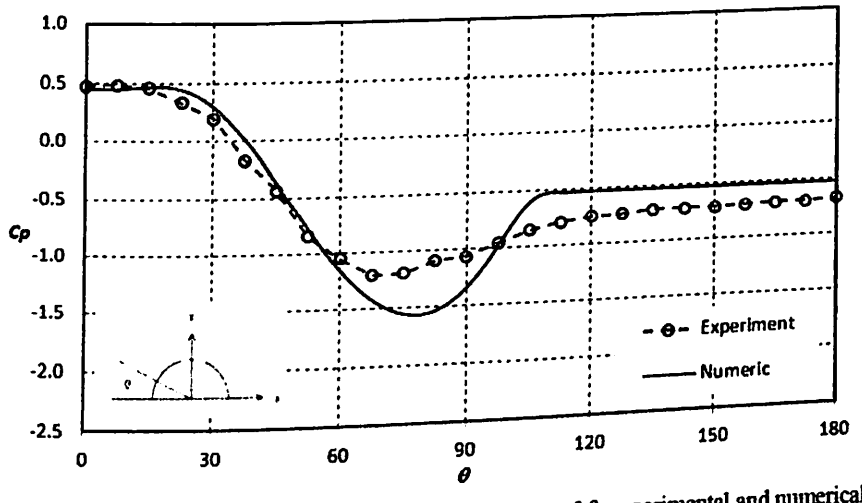

FIGURE 5. The distribution of Cp in bumps without wire as a function of θ: experimental and numerical results.

Figure 6 shows the distribution of Cp in bumps with and without tripping wire obatined from numerical simulations. From the Fig. 6, it can be seen that all four graphs have the same or similar tendency in the range of $0° \leq \theta \leq 30°$. When the flow passes the transversal wire, the flow experiences sudden pressure drop and the most extreme drop is for the wire located at $\theta = 50°$, compared to the other wire locations seem to be related with the location of the local reattachment points of the flow after it separated from the tripping wire. Beyond to $\theta = 180°$, the effect of the tripping wire is not appeared, indicated by the overlapping data from all the wire locations, i.e., $\theta = 30°$, 40°, and 50°. In the range of $105° \leq \theta \leq 180°$, the four graphs back to have the same tendency, indicated that the flow characteristics are the same for all four cases.

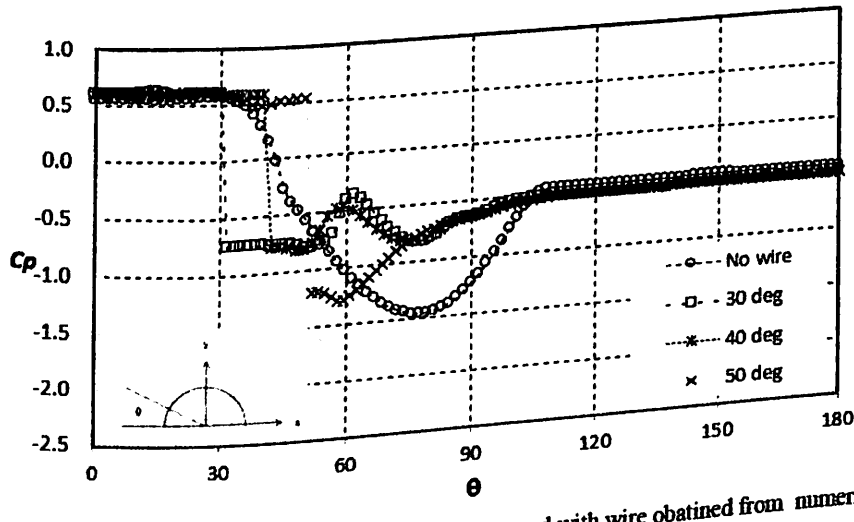

FIGURE 6. Pressure distribution (Cp) on the bump surface without and with wire obatined from numerical simulations.

Figure 7 shows the distribution of Cp in bumps with and without tripping wire obatined from experiments. From the Fig. 7, it can be seen that all four graphs have the same or similar tendency in the range of $0° \leq \theta \leq 15°$. When the flow passes the transversal wire, the flow experiences sudden pressure drop and the most extreme drop is for the wire located at $\theta = 50°$, compared to the other wire locations. In the range of $80° \leq \theta \leq 180°$, the four

graphs back to have the same tendency, but the tripping wire (disturbance rod) located at $\theta = 40°$ has the largest Cp value, while the bump without the transversal wire has the smallest Cp value.

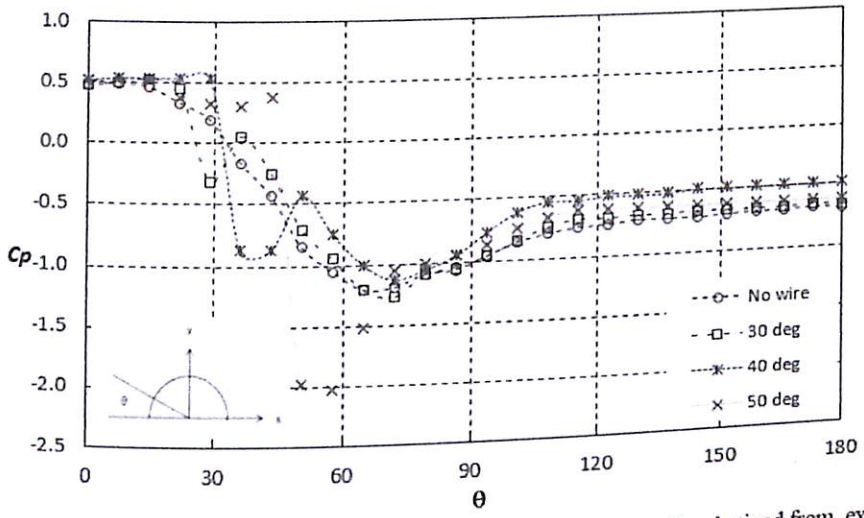

FIGURE 7. Pressure distribution (Cp) on the bump surface without and with wire obatined from experiments.

Figures 8 and 9 show the velocity profiles from the experimental and numerical results, repectively, along a flat plate with a semicircular bump. Velocity profiles are taken at 8 sections with a range of $-3 < x/d < 8$ and the distance between profile location is one bump diameter and measured as far as 10 cm from the plate with a vertical distance between points of 1 mm. In Fig. 9, the velocity profile obtained from the numerical simulation plotted along the flat plate with a bump at 13 sections with a spacing between sections of $1d$, where d is the bump diameter. Figures 8 and 9 show that the flow is accelerated before approaching the bump midspan at the outside of the boundary layer. This acceleration is shown by the value of u/U increases in the direction of the flow. When the flow passes through the bump apex, the flow attains its maximum velocity, due to the reduction in cross-sectional area above the bump. The maximum velocity is approximately $u_{max}/U = 1.28$.

As the flow goes downstream, the separated area becomes smaller, and eventually the velocity profile backs to normal condition without any separated region. The point at which the flow returns to normal is called the reattachment point. From Fig. 8 it can be seen that the reattachment point of the downstream of the bump without wire occurs at $x \sim 4.0d$, while from Fig. 9, it can be seen that the reattachment point of the flow over the bump without wire occurs at $x \sim 3.5d$. Experimental and numerical results show slight difference reattachment point position. The difference is, howerver, not too significant, and this difference is probably due to the total pressure tube reading experimental uncertainty.

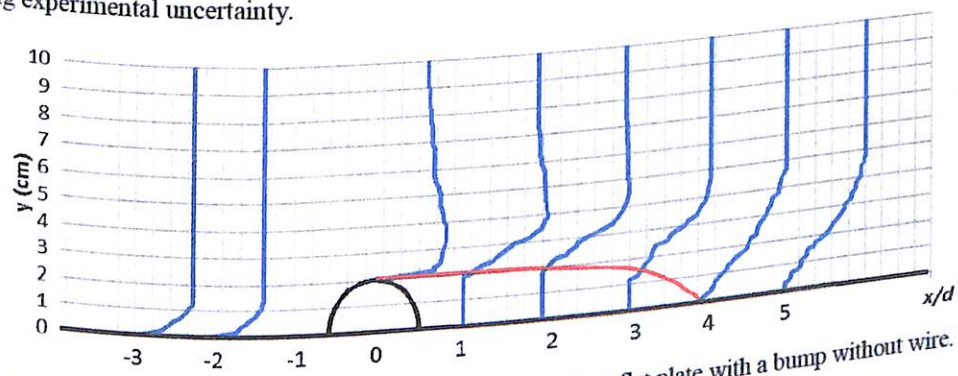

FIGURE 8. Experimental results of velocity profiles (m/s) on flat plate with a bump without wire.

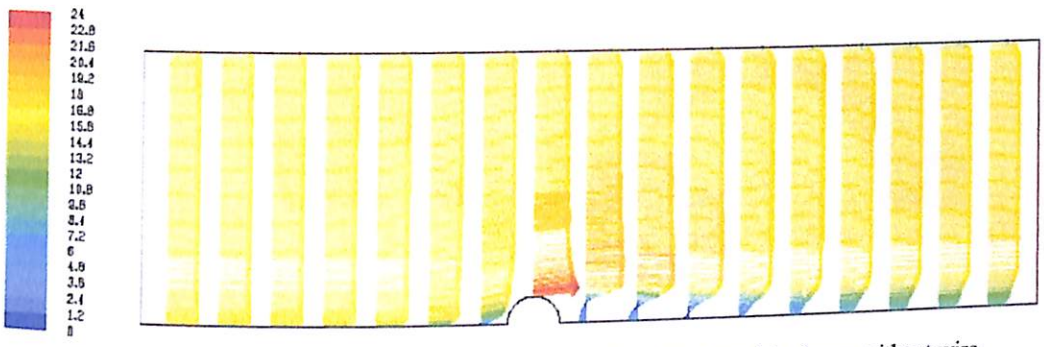

FIGURE 9. Numerical results of velocity profiles (m / s) on flat plate with a bump without wire.

Figure 10 shows the velocity profiles from the experimental results measured along a flat plate with a semicircular bump with tripping wire located at $\theta = 50°$, while Fig. 11 shows the velocity profiles for the same geometry but obtained from the simulation. Similar flow development over the bump with tripping wire almost the same as that develops over the bump without the wire. From the numerical results, it is shown that the maximum velocity is, however, slightly smaller for the flow over the bump with tripping wire, i.e. $u_{max}/U = 1.24$, or approximately 3 percent smaller than that over the bump without tripping wire. This reduction in the is probably due to the wake formation just behind of the tripping wire.

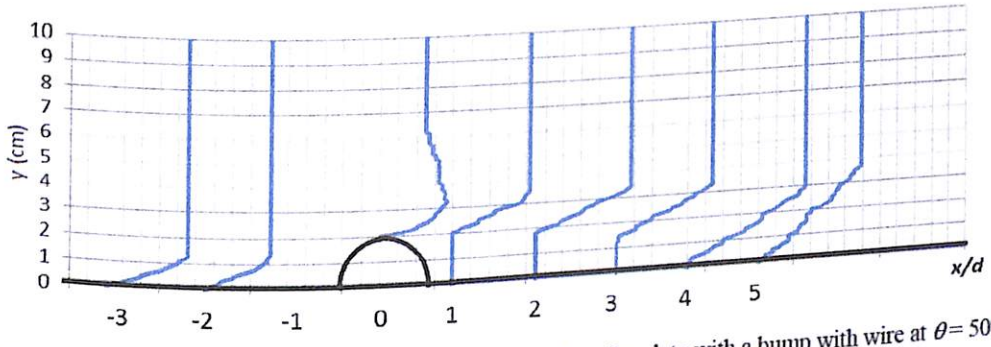

FIGURE 10. Experimental results of velocity profiles (m/s) on flat plate with a bump with wire at $\theta = 50°$.

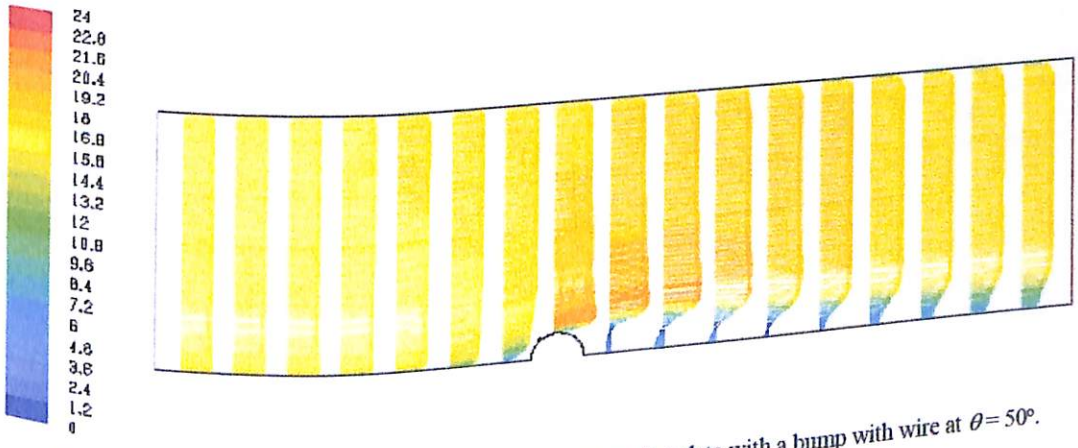

FIGURE 11. Numerical results of velocity profiles (m/s) on flat plate with a bump with wire at $\theta = 50°$.

The separation point can be seen better from the velocity streamlines as shown in Fig. 12. After passing the bump, the flow slows down so that the velocity returns to normal condition. The flow separation point from the bump occurs at an angle just downstream of the bump midspan, i.e. at $\theta \sim 110°$ in the case of bump without tripping wire, where its separation moves forward as the tripping wire is added on the bump.

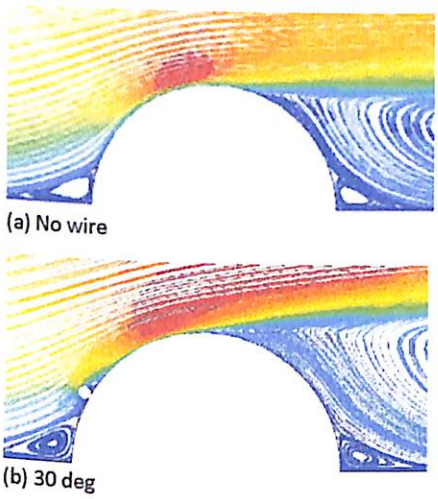

FIGURE 12. Flow streamline contour on the bump surface obtained from numerical study: (a) without tripping wire; (b) wire at 30o; (c) wire at 50o.

Table 2 shows the drag coefficient (C_D) of the flat plate with a bump, with and without tripping wire. There are three drag values: pressure drag ($C_{D,p}$), friction or viscous drag ($C_{D,f}$), and total drag ($C_{D,T}$), which is the sum of the pressure and friction drags. Table 2 also shows the results obtained from numerical simulation as well as from the experiments.

Figure 13 shows comparison of the drag coefficients on the bump with and without tripping wire obtained experimentally and numerically. From the Fig. 13, it can be seen that the drag coefficients of the bump with tripping wire have similar results, either obtained numerically or experimentaly. In average, the results obtained experimentaly are slightly higher than that obtained numerically, with the maximum difference between experimental and numerical results is approximately 5% at $\theta = 50°$. Bump with tripping wire produces drag higher than that for without tripping wire. The increase in drag is up to approximately 50 percent for wire intallation at $\theta = 50°$. C_D for reference line means that the drag coefficient for the bump without the tripping wire.

TABLE 2. Drag coefficient (C_D) of the flat plate with a semi-circular bump, with and without wire.

Flat Plate with Bump and wire Location	Experiment			Numeric		
	$C_{D,p}$	$C_{D,f}$	$C_{D,T}$	$C_{D,p}$	$C_{D,f}$	$C_{D,T}$
No-wire	0.619	0.492	1.111	0.900	0.218	1.118
30 deg	0.629	0.948	1.577	1.333	0.176	1.509
40 deg	0.428	1.081	1.509	1.340	0.165	1.505
50 deg	0.493	1.196	1.690	1.497	0.147	1.644

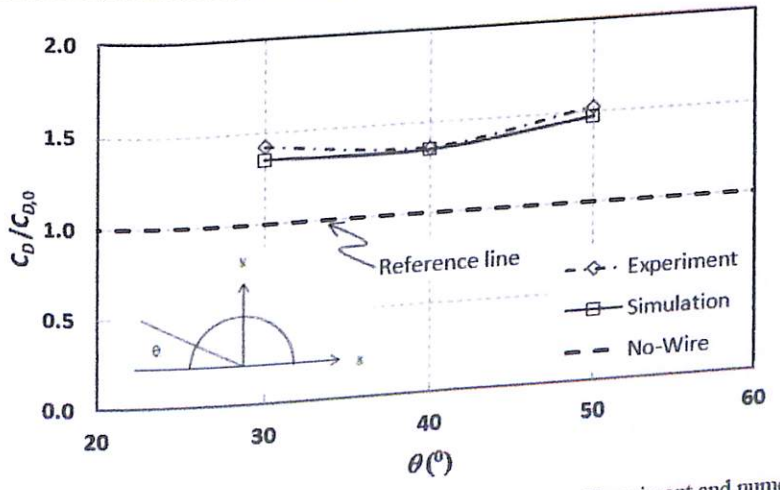

FIGURE 13. Drag coefficient (C_D) of bump without and with tripping wire. Experiment and numerical simulation.

CONCLUSIONS

Some conclusions that can be drawn from this study include:

1. The presence of the tripping wire on the upstream surface of the semi-circular bump increases the total drag coefficient (C_D).
2. The addition of tripping wire / rods on the bump surface advances the point of the boundary layer separation.
3. Experimental data and numerical simulation results show similar values in the total drag coefficients with a maximum difference of approximately 5%.

REFERENCES

1. W. Wijanarko, Separasi dan Reattachment Aliran di Belakang Gundukan (Bump) Setengah Lingkaran, Segitiga, dan Persegi Panjang. Tugas Akhir, Teknik Mesin ITS, Surabaya (2005).
2. K. Joongnyon and J.S. Hyung, Wall Pressure Fluctuations in a Turbulent Boundary Layer over a Bump. Korea Advanced Institute of Science and Technologi, Republic of Korea (2006).
3. H.S. Hadi, Studi Eksperimen dan Numerik Tentang Aliran Boundary Layer yang Melintasi "Bump" dengan Radius Kelengkungan yang Kecil. Tugas Akhir, Teknik Mesin ITS, Surabaya (2011).
4. H. Werlé, (ONERA), in "An Album of Fluid Motion," (Van Dyke, Parabolic Press, 1982).
5. N.J. Mulvany, L. Chen, J.Y. Tu, and B. Anderson, Steady-State Evaluation of 'Two-Equation' RANS (Reynolds-averaged Navier-Stokes) Turbulence Models for High-Reynolds Number Hydrodynamic Flow Simulations. (DSTO Platform Sciences Laboratory 506 Lorimer St.Fishermans Bend, Victoria 3207 Australia, 2004).